

Manipulating the electronic structure and superconductivity of Li_2B_3C by biaxial strain

Yuhao Gu(顾雨豪), Yihao Wang(王奕淏), and Shuxian Hu(胡淑贤)

Citation: Chin. Phys. B, 2026, 35 (**4**): 047401. DOI: 10.1088/1674-1056/ae5594
http://cpb.iphy.ac.cn; http://iopscience.iop.org/cpb

What follows is a list of articles you may be interested in

A semiconductor-like in-plane junction between overdoped and optimally doped $La_{2-x}Ce_xCuO_4$

Mohsin Rafique(莫辛 拉菲克), Rui Wu(吴蕊), Zefeng Lin(林泽丰), Kui Jin(金魁), Qi-Kun Xue(薛其坤), and Ding Zhang(张定)

Chin. Phys. B, 2025, 34 (**9**): 097404. DOI: 10.1088/1674-1056/adda09

Superconductivity and band topology of double-layer honeycomb structure M_2N_2 (M = Nb, Ta)

Jin-Han Tan(谭锦函), Na Jiao(焦娜), Meng-Meng Zheng(郑萌萌), Ping Zhang(张平), and Hong-Yan Lu(路洪艳)

Chin. Phys. B, 2025, 34 (**9**): 097402. DOI: 10.1088/1674-1056/adee04

Superconductivity in YbN_4H_{12} under low pressures

Xiang Wang(汪翔), Chenlong Xie(谢晨龙), Haohao Hong(洪浩豪), Yanliang Wei(魏衍亮), Zhao Liu(刘召), and Tian Cui(崔田)

Chin. Phys. B, 2025, 34 (**8**): 087401. DOI: 10.1088/1674-1056/add908

Theoretical investigation of potential superconductivity in Sr-doped $La_3Ni_2O_7$ at ambient pressure

Lei Shi(石磊), Ying Luo(罗颖), Wei Wu(吴为), and Yunwei Zhang(张云蔚)

Chin. Phys. B, 2025, 34 (**7**): 077403. DOI: 10.1088/1674-1056/add1bd

Phonon-mediated superconductivity in orthorhombic XS (X = Nb, Ta or W)

Guo-Hua Liu(刘国华), Kai-Yue Jiang(江恺悦), Yi Wan(万一), Shu-Xiang Qiao(乔树祥), Jin-Han Tan(谭锦函), Na Jiao(焦娜), Ping Zhang(张平), and Hong-Yan Lu(路洪艳)

Chin. Phys. B, 2025, 34 (**2**): 027401. DOI: 10.1088/1674-1056/ad9733

RAPID COMMUNICATION

Manipulating the electronic structure and superconductivity of Li_2B_3C by biaxial strain

Yuhao Gu(顾雨豪)[†,‡], Yihao Wang(王奕淏)[†], and Shuxian Hu(胡淑贤)[§]

School of Mathematics and Physics, University of Science and Technology Beijing, Beijing 100083, *China*

(Received 8 March 2026; revised manuscript received 20 March 2026; accepted manuscript online 23 March 2026)

Strain is a clean and efficient method to manipulate physical properties without changing the chemical composition. In this paper, we perform a systematic first-principles study of how biaxial strain manipulates the electronic structure and phonon-mediated superconductivity of Li_2B_3C with its optimal configuration. Here we introduce a descriptor $\Delta\varepsilon$, defined as the energy offset between the B–B bridge σ-bonding band maximum and the Fermi level. We screen the biaxial-strained Li_2B_3C structures in the range of -5% to $+5\%$ and retain those with $\Delta\varepsilon > 0.05$ eV for subsequent electron-phonon coupling (EPC) calculations. The maximum $T_c = 44.72$ K occurs at $+5\%$ *a*-axis strain and -5% *b*-axis strain. We then elucidate the microscopic mechanism underlying the strain response of the electronic structure by analyzing the corresponding changes of the structure and tight-binding parameters. Taking the optimal biaxial-strained Li_2B_3C as an example, we analyze its phonon properties and discuss the origin of its strong EPC. Our work provides reliable theoretical guidance for manipulating electronic structure and superconductivity by strain, and sheds new light on high-T_c superconductivity induced by metallic σ-bonding electrons.

Keywords: electronic structure, phonon-mediated superconductivity, first-principles calculation, biaxial strain

PACS: 74.20.Pq, 63.20.kd, 74.20.Fg, 71.15.Mb

DOI: 10.1088/1674-1056/ae5594 **CSTR:** 32038.14.CPB.ae5594

1. Introduction

The search for new superconductors with higher T_c remains a central objective in condensed matter physics and materials science. According to Bardeen–Cooper–Schrieffer theory, phonon-mediated superconductivity is naturally promoted by high characteristic phonon frequencies. As a result, it is natural to explore materials composed of light elements. This motivation is first epitomized by the long-standing pursuit of metallic hydrogen.[1] Furthermore, great progress has been made in hydrogen-rich compounds such as H_3S[2,3] and LaH_{10}.[4,5]

Another route to enhance T_c is to increase the EPC strength. One effective strategy is the metallization of σ-bonding electrons.[6–8] A σ-bond is the strongest covalent bond, formed by two head-on orbitals. As a result, σ states naturally couple strongly with the lattice. However, the σ-bonding/antibonding states are often situated far below/above the Fermi level owing to its strong covalent hybridization. As discussed in Refs. [7,9], one can usually metallize those σ-bonding electrons by external pressure, charge doping or crystal-field effect. The 39 K superconductivity in MgB_2 is a textbook example of the strategy that uses the crystal-field effect.[6,10,11] In MgB_2, the Mg^{2+} ions strongly attract the π electrons in the boron layers, lowering the energy of the π-bands. Relatively, the energies of the in-plane σ-bands are raised and their band top crosses the Fermi level.

Inspired by the success of MgB_2, researchers attempted to explore other materials with metallic σ-bonding electrons.[8,12–21] LiBC is structurally similar and isoelectronic with MgB_2. Therefore, theorists predicted that hole-doped $Li_{1-x}BC$ could exhibit metallic σ-bonding electrons and lead to high transition temperatures.[12,13] However, experimental evidence shows that finite lithium deficiencies cannot stabilize the predicted crystal structure, precluding the metallization of σ-bonding electrons.[22–28]

To alleviate the lattice instability associated with Li deficiency, Gao *et al.* proposed introducing holes via partial B-for-C substitution in LiBC.[7,8] Based on first-principles calculations, they identified two promising superconducting candidates, Li_2B_3C ($n = 2$) and $Li_3B_4C_2$ ($n = 3$), with predicted T_c values exceeding 50 K. Related substitution-based strategies were later proposed by other groups.[14–16] However, the atomic configuration of B and C atoms, known as "the coloring problem",[29,30] has been overlooked in previous studies of $LiB_{1+x}C_{1-x}$.[31]

To address this issue, Gu *et al.* investigated the stable configurations of Li_2B_3C and $Li_3B_4C_2$ using the cluster expansion method.[31] They identified that the energetically stable configurations are characterized by a distinctive pattern of alter-

[†]These authors contributed equally to this work.

[‡]Corresponding author. E-mail: guyuhao@ustb.edu.cn

[§]Corresponding author. E-mail: hushuxian@ustb.edu.cn

© 2026 Chinese Physical Society and IOP Publishing Ltd. All rights, including for text and data mining, AI training, and similar technologies, are reserved.

nating B–B and B–C zigzag chains. Moreover, these structures exhibit low superconducting transition temperatures, e.g., $T_c <$ 0.03 K in Li_2B_3C. However, a -5% compressive b-axial strain can remarkably enhance the EPC, boosting T_c to 37 K.

In this paper, we present a systematic first-principles study of how biaxial strain manipulates the electronic structure and phonon-mediated superconductivity of Li_2B_3C with its optimal configuration. Firstly, we perform the structural relaxations and electronic structure calculations for Li_2B_3C under different biaxial strains in the moderate range of -5% to $+5\%$ at the DFT level. Inspired by our previous study,[31] we introduce a simple descriptor, $\Delta\varepsilon$, defined as the energy difference between the B–B bridge σ-bonding band maximum and E_F. Using $\Delta\varepsilon > 0.05$ eV as a screening criterion, we carry out subsequent EPC calculations. For the selected structures, T_c ranges from 14 K to 45 K. The maximum $T_c = 44.72$ K occurs at $+5\%$ a-axis strain and -5% b-axis strain, with the strongest EPC strength ($\lambda = 1.13$) and the slightly reduced logarithmic average phonon frequency ($\omega_{log} = 46.69$ meV). Furthermore, we find that b-axis compression or a-axis tension is beneficial to lift up the B–B bridge σ-bonding band maximum. Combining the analysis of tight-binding (TB) parameters, we elucidate the detailed mechanism of how strain tunes the electronic structure. Finally, we analyze the EPC properties of the optimal biaxial-strained Li_2B_3C. We find that its strong EPC originates from its elliptical cylindrical Fermi surfaces around Γ point, composed of states with large deformation potentials.

2. Computational methods

We employ Quantum ESPRESSO[32] to carry out the DFT calculations. We adopt the PBE exchange–correlation functional[33] and the SG15 norm-conserving pseudopotentials.[34–36] To simulate biaxial strains, the c-axis and atomic coordinates of Li_2B_3C are fully relaxed while in-plane lattice constants are fixed. The energy convergence criterion is 10^{-12} Ry and the force convergence criterion is 10^{-6} Ry/Bohr. The kinetic energy cutoff is set to 80 Ry and the $\boldsymbol{k}$-grid is $16\times8\times6$. The Marzari–Vanderbilt–DeVita–Payne smearing method[37] is employed with a smearing of 0.015 Ry.

We employ Wannier90[38,39] to calculate maximally localized Wannier functions (MLWFs) for analyzing electronic structures. The energy window and frozen window for the disentanglement procedure in Wannierization are -16.04 eV to 11.08 eV and -16.04 eV to 0.00 eV, respectively. The Wannier centers are set on B/C atoms for p_z-like Wannier functions (WFs) and on B–B/B–C bond centers for s-like B–B/B–C bonding WFs.

We employ EPW package[40,41] to calculate the EPC properties. We take the $16\times8\times6$ $\boldsymbol{k}$-mesh and $8\times4\times3$ $\boldsymbol{q}$-mesh as coarse grids and then interpolate them to the dense $64\times32\times24$ $\boldsymbol{k}$-mesh and $16\times8\times6$ $\boldsymbol{q}$-mesh in Li_2B_3C, respectively. The Gaussian smearing method with a width of 0.05 eV is used for the Fermi surface broadening.

The superconducting transition temperature T_c is calculated with the McMillan–Allen–Dynes formula[42,43]

$$T_c = \frac{\omega_{log}}{1.2}\exp\left[\frac{-1.04(1+\lambda)}{\lambda(1-0.62\mu^*)-\mu^*}\right]. \tag{1}$$

Here λ is the total EPC strength, μ^* is the effective screened Coulomb pseudopotential, and ω_{log} is the logarithmic average of the Eliashberg spectral function. λ and ω_{log} are defined as

$$\lambda = \sum_{q\nu}\lambda_{q\nu} = 2\int\frac{\alpha^2F(\omega)}{\omega}\mathrm{d}\omega, \tag{2}$$

$$\omega_{log} = \exp\left[\frac{2}{\lambda}\int\frac{\mathrm{d}\omega}{\omega}\alpha^2F(\omega)\ln(\omega)\right], \tag{3}$$

$$\alpha^2F(\omega) = \frac{1}{2}\sum_{q\nu}\delta(\omega-\omega_{q\nu})\omega_{q\nu}\lambda_{q\nu}. \tag{4}$$

Here $\omega_{q\nu}$ and $\lambda_{q\nu}$ are the frequency and EPC strength of the ν-th phonon mode at the wave vector $\boldsymbol{q}$. The $\lambda_{q\nu}$ is defined as

$$\lambda_{q\nu} = \frac{\gamma_{q\nu}}{\pi\hbar N(0)\omega_{q\nu}^2}. \tag{5}$$

Here $\gamma_{q\nu}$ is the phonon linewidth:

$$\begin{aligned}\gamma_{q\nu} &= 2\pi\omega_{q\nu}\sum_{i,j}\int\frac{\mathrm{d}\boldsymbol{k}}{\Omega_{BZ}}|g_{q\nu}(\boldsymbol{k},i,j)|^2\\ &\quad\times\delta(\varepsilon_{\boldsymbol{k},i}-\varepsilon_F)\delta(\varepsilon_{\boldsymbol{k}+\boldsymbol{q},j}-\varepsilon_F).\end{aligned} \tag{6}$$

Here i/j is the band index. The electron–phonon interaction matrix element $g_{q\nu}(\boldsymbol{k},i,j)$, describing the probability amplitude for scattering of an electron with a transfer of crystal momentum $\boldsymbol{q}$, is determined by

$$\begin{aligned}g_{q\nu}(\boldsymbol{k},i,j) &= \sqrt{\frac{\hbar}{2\omega_{q\nu}}}\langle\psi_{\boldsymbol{k},i}|\Delta V_{KS}^{q\nu}|\psi_{\boldsymbol{k}+\boldsymbol{q},j}\rangle;\\ \Delta V_{KS}^{q\nu} &= \sum_{\boldsymbol{R},s}\frac{\partial V_{KS}}{\partial u_{s\boldsymbol{R}}}u_s^{q\nu}\frac{\mathrm{e}^{\mathrm{i}\boldsymbol{q}\boldsymbol{R}}}{\sqrt{N}}.\end{aligned} \tag{7}$$

Here $u_s^{q\nu} = \nu_s^{q\nu}/\sqrt{M_s}$ and $\partial V_{KS}/\partial u_{s\boldsymbol{R}}$ can be calculated by density functional perturbation theory (DFPT).[44]

3. Results and discussion

3.1. The biaxial strain

The crystal structure of Li_2B_3C with its optimal configuration[31] is shown in Fig. 1(a), belonging to the orthorhombic crystal system. In our previous work, we demonstrated that b-axis uniaxial strain can effectively tune the electronic structure and enhance T_c. However, when we apply uniaxial strain, the lattice constants along the other two directions relax simultaneously. These coupled structural responses complicate a clean interpretation of the evolution of the electronic structure. Therefore, in this study, we investigate the electronic structure and superconducting properties of Li_2B_3C

under biaxial strain in the range of −5% to +5%. In the simulation of the biaxial strain, we fix the in-plane lattice constants a and b, and relax the out-of-plane lattice constant c. Because Li_2B_3C has a layered structure, variation in the out-of-plane lattice constant c has only a minor impact on its electronic structure, as detailed in the supporting information (SI).

According to the conclusion of our previous study,[31] the key of enhancing T_c in Li_2B_3C is the metallization of the B–B bridge σ-bonding band, thereby activating the large — deformation-potential states near its band maximum effectively. Hence, we define the descriptor, $\Delta\varepsilon$, as the energy separation between the band maximum of the B–B bridge σ-bonding band and the Fermi level, as illustrated in Fig. 1(b). When $\Delta\varepsilon > 0$, the B–B bridge σ-bonding band crosses E_F; conversely, $\Delta\varepsilon < 0$ indicates that this band maximum remains below the Fermi level. Moreover, a larger $\Delta\varepsilon$ also implies a larger Fermi surface and larger density of states (DOS) at the Fermi level, which is beneficial for enhancing the total EPC.

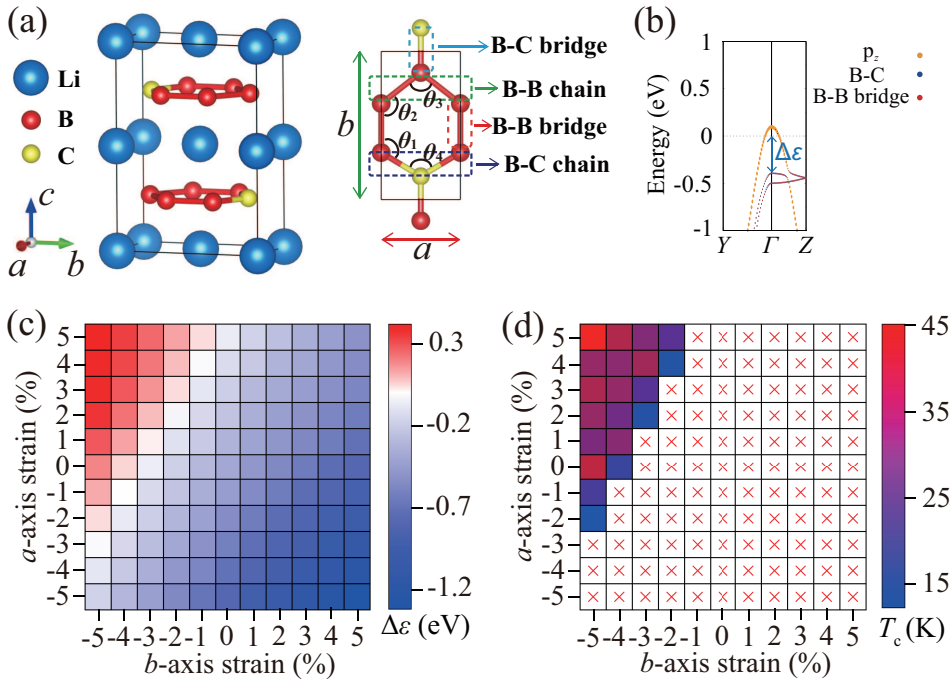


Fig. 1. (a) The crystal structure of Li_2B_3C with the optimal configuration. B–C bridge bonds, B–B zigzag chains, B–B bridge bonds and B–C zigzag chains are marked by light blue, green, red and dark blue frames in the B_3C layer, respectively. The bond angles θ_{1-4} are also labeled in the B_3C layer. (b) The schematic illustration of the descriptor $\Delta\varepsilon$. Here we take the band structure of Li_2B_3C without strain as an example. (c) Map of $\Delta\varepsilon$ under biaxial strains. (d) Map of superconducting transition temperature T_c under biaxial strains when $\Delta\varepsilon > 0.05$ eV. Phases with $\Delta\varepsilon < 0.05$ eV are labeled with crosses.

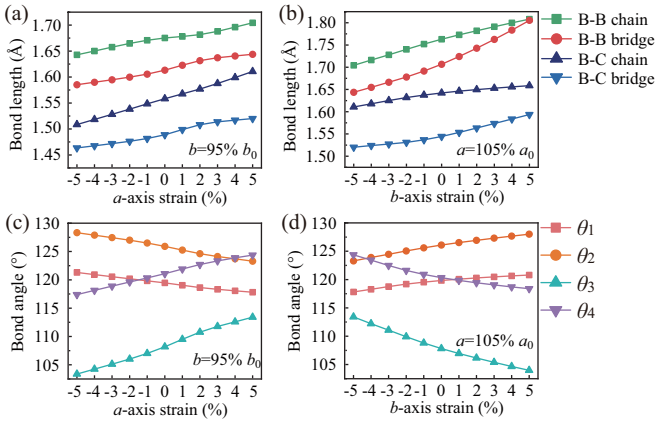


Fig. 2. (a) The variation of different bond lengths in Li_2B_3C as a function of a-axis strain when b-axis strain is fixed at −5%. (b) The variation of bond lengths in Li_2B_3C as a function of b-axis strain when a-axis strain is fixed at +5%. (c) The variation of bond angles in Li_2B_3C as a function of a-axis strain when b-axis strain is fixed at −5%. (d) The variation of bond angles in Li_2B_3C as a function of b-axis strain when a-axis strain is fixed at +5%.

We calculate the electronic structure of Li_2B_3C and the associated descriptor $\Delta\varepsilon$ across a biaxial strain window of −5% to +5%, as shown in Fig. 1(c). The results show that b-axis compressive strain and a-axis tensile strain are both effective in enlarging $\Delta\varepsilon$, i.e., pushing the B–B bridge σ-bonding band across the Fermi level. Considering the positive correlation between $\Delta\varepsilon$ and T_c, we choose $\Delta\varepsilon > 0.05$ eV as a screening criterion. We carry out EPC calculations for the selected structures, as shown in Fig. 1(d). All selected structures exhibit sizable T_c values (at least 14 K), confirming the validity of our choice of descriptor.

In Li_2B_3C, the B_3C layers are formed by assemblies of alternating B–B and B–C zigzag chains, thereby minimizing the electronic energy.[31] Thus, we denote the bond inside the zigzag chain "chain bond", and denote the bond between two zigzag chains "bridge bond", as illustrated in Fig. 1(a). The simulation of biaxial strain allows us to isolate the effect of varying one in-plane lattice constant on the structure while keeping the other fixed, as shown in Fig. 2. Here we use $b = 95\%b_0$ and $a = 105\%a_0$ as two examples. As shown in Figs. 2(a) and 2(b), all in-plane bond lengths

increase/decrease with increasing tensile/compressive strain along the scanned axis. In particular, at large strain magnitude, the tensile/compressive a-axis strain induces a more pronounced elongation/contraction of the chain bonds, whereas b-axis strain preferentially stretches the bridge bonds, consistent with the lattice geometry.

Moreover, the bond angle is another crucial in-plane structural parameter because it directly modulates orbital overlap along the covalent network. As shown in Fig. 1(a), we label $\theta_{1,2}$ as the angles between a chain bond and a bridge bond, and $\theta_{3,4}$ as the angles between two chain bonds. When applying the epitaxial strain, the angular degrees of freedom provide the dominant structural compensation. The bond angles show two opposite trends. Under a-axis tension or b-axis compression, the B–B and B–C zigzag chains are stretched. Thus, $\theta_{1,2}$ decrease and $\theta_{3,4}$ increase, as depicted in Fig. 2(c). As a result, the anticorrelated evolution of the bond angles provides a handle to tune the electronic structure.

3.2. The electronic structure

Epitaxial strain provides an effective and clean route to tune the physical properties of a material without changing its chemical composition.[45–51] The projected band structures and DOS for Li_2B_3C under different biaxial strains are shown in Fig. 3. To distinguish the contributions from chain bonds and bridge bonds in the band structure, we project the bands onto the WFs centered on chain bonds and bridge bonds. Without strain, only the π bands and B–B zigzag chain σ-bonding bands intersect the Fermi level in Li_2B_3C. Clearly, the band maximum of the B–B bridge σ-bonding band is lifted up under a-axis tension and b-axis compression. As a result, the B–B bridge σ-bonding band (the red band) intersects the Fermi level under tensile a-axis strain and compressive b-axis strain, as marked by dashed purple circles in Figs. 3(a) and 3(d). In addition, from the results of DOS, we can observe strong hybridization between B–B and B–C bridge σ-bonding WFs near the maximum of B–B bridge σ-bonding band. Notably, the B–B zigzag chain σ-bonding band (the green band) exhibits an opposite response to strain.

In a single particle picture, the electronic structure can be quantitatively described by the TB Hamiltonian, which can be written as

$$H_{\mathrm{TB}} = \sum_{\boldsymbol{k}\alpha} \varepsilon_\alpha C^\dagger_{\boldsymbol{k}\alpha} C_{\boldsymbol{k}\alpha} + \sum_{\boldsymbol{k},\alpha\neq\beta} \mathrm{e}^{\mathrm{i}\boldsymbol{k}R_{\alpha\beta}} t_{\alpha\beta} C^\dagger_{\boldsymbol{k}\alpha} C_{\boldsymbol{k}\beta}, \tag{8}$$

where ε_α denotes the on-site energy, $t_{\alpha\beta}$ denotes the hopping parameter. In order to quantify the response of electronic structure under biaxial strain, we analyze the TB parameters, the on-site energies ε_α and the nearest-neighboring

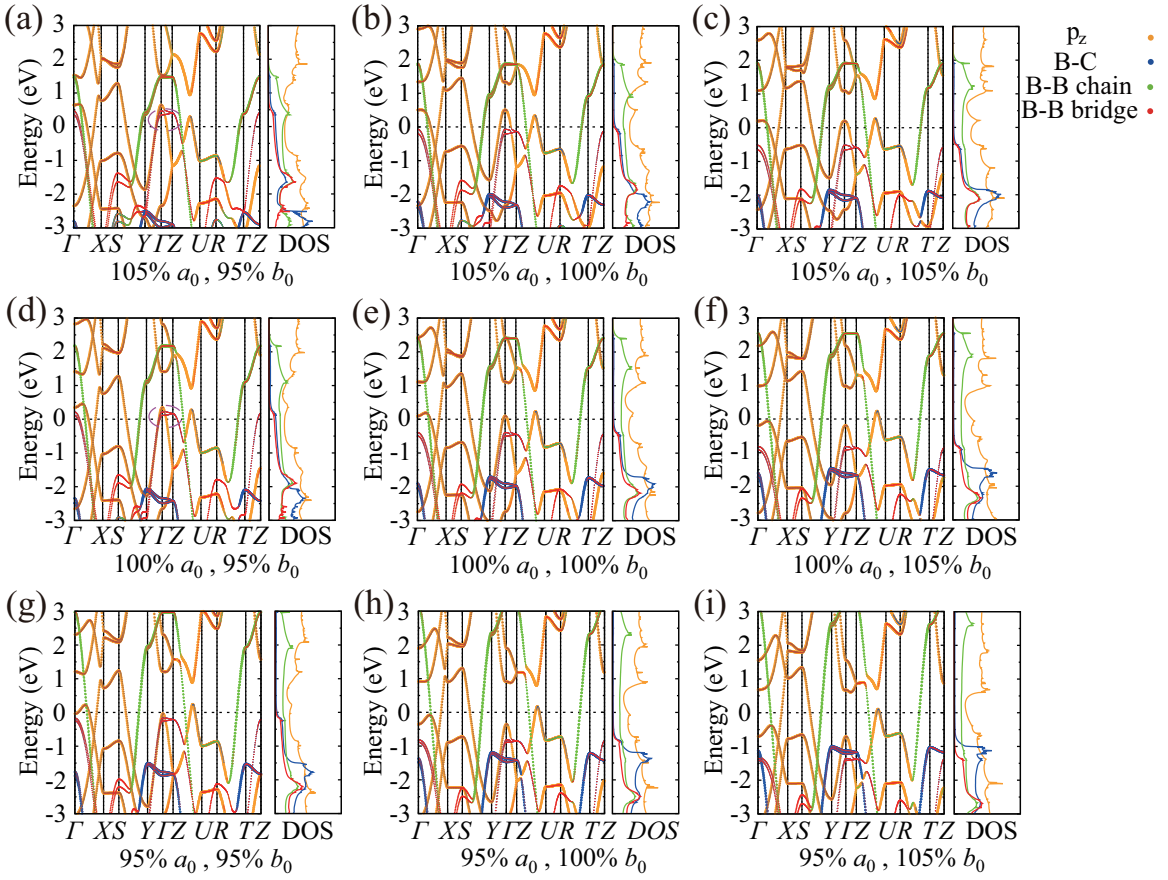


Fig. 3. The projected band structures and the corresponding projected DOS for Li_2B_3C under different biaxial strains. The dot sizes are proportional to the spectral weights obtained from Wannierization. The tops of the bridge site σ-bonding bands near the Γ point, which are sensitive to phonon vibrations, are marked by dashed purple circles. The high-symmetry $\boldsymbol{k}$-points are the same as those in Ref. [31].

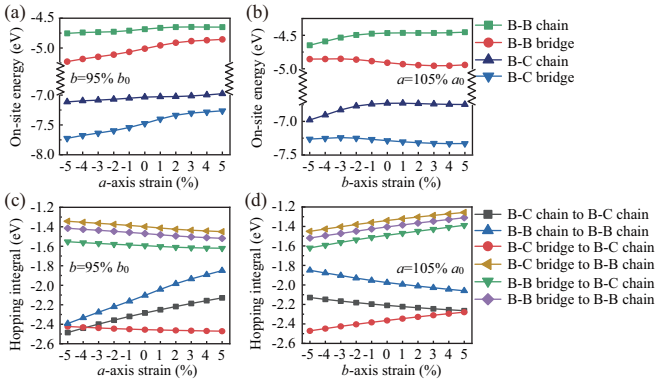


Fig. 4. (a) The variation of on-site energies of σ-bonding WFs in Li_2B_3C as a function of a-axis strain when b-axis strain is fixed at -5%. Here E_F is set to 0. (b) The variation of on-site energies of σ-bonding WFs in Li_2B_3C as a function of b-axis strain when a-axis strain is fixed at $+5\%$. (c) The variation of NN hopping parameters between σ-bonding WFs in Li_2B_3C as a function of a-axis strain when b-axis strain is fixed at -5%. (d) The variation of NN hopping parameters between σ-bonding WFs in Li_2B_3C as a function of b-axis strain when a-axis strain is fixed at $+5\%$.

hopping integrals $t_{\alpha\beta}$, extracted from Wannierization. As in the structural analysis, we vary one in-plane lattice constant while holding the other fixed. As shown in Figs. 4(a) and 4(b), both a-axis tension and b-axis compression increase the on-site energy of B–B bridge σ-bonding WF (E_F is set as 0). In other words, such strains can raise the band center of B–B bridge σ-bonding band.

On the other hand, the variation of hopping strength plays a more important role in raising the band maximum of B–B bridge σ-bonding band. As shown in Figs. 4(c) and 4(d), a-axis tension or b-axis compression reduces the magnitudes of intra-chain hoppings but enhances the magnitudes of bridge-chain hoppings. Such behavior originates from the corresponding structural response. Under a-axis tension or b-axis compression, the zigzag chain is stretched. Accordingly, $\theta_{1,2}$ decrease, while $\theta_{3,4}$ increase. This weakens the intra-chain hybridization but strengthens the bridge-chain hybridization. Consequently, a-axis tension or b-axis compression relatively broadens the B–B bridge σ-bonding band, which facilitates pushing its band maximum above the Fermi level. So far, we elucidate the detailed mechanism of how strain manipulates the electronic structure of Li_2B_3C.

3.3. The electron–phonon coupling

According to our previous study,[31] the Lifshitz transition induced by strain triggers the enhancement of T_c in Li_2B_3C. In this work, we perform subsequent EPC calculations for all biaxial-strained structures satisfying $\Delta\varepsilon > 0.05$ eV, as detailed in our SI. Table S1 shows that, for all structures with $\Delta\varepsilon > 0.05$ eV (using $\mu^* = 0.10$), T_c ranges from 14 K to 45 K. The maximum $T_c = 44.72$ K occurs at $+5\%$ a-axis strain and -5% b-axis strain, where the EPC is strongest ($\lambda = 1.13$) despite a reduced logarithmic average phonon frequency ($\omega_{log} = 46.69$ meV). This T_c value is higher than the one under the uniaxial strain,[31] and above the McMillan limit. In addition, we find that a-axis tension and b-axis compression significantly enhance the EPC strength, although they slightly reduce ω_{log}. Overall, the gain in EPC outweighs the modest decrease in ω_{log}, leading to the enhancement of T_c.

The phonon band dispersions and the corresponding EPC strengths $\lambda_{q\nu}$ for Li_2B_3C without strain and with optimal biaxial strain are given in Figs. 5(a) and 5(c). Compared with the strain-free case, the EPC strength and the corresponding Eliashberg spectral function for Li_2B_3C under the optimal biaxial strain are significantly enhanced (the marker sizes in panel (a) are doubled for aesthetic visualization), although the phonon frequencies slightly decrease. For both cases, the phonon mode with the strongest EPC is the bond-stretching A_g mode, as marked in Figs. 5(a) and 5(c). In addition, the Kohn-anomaly-like phonon softenings near 20 meV along the Γ–X and Z–U lines make sizable contributions to the total EPC.

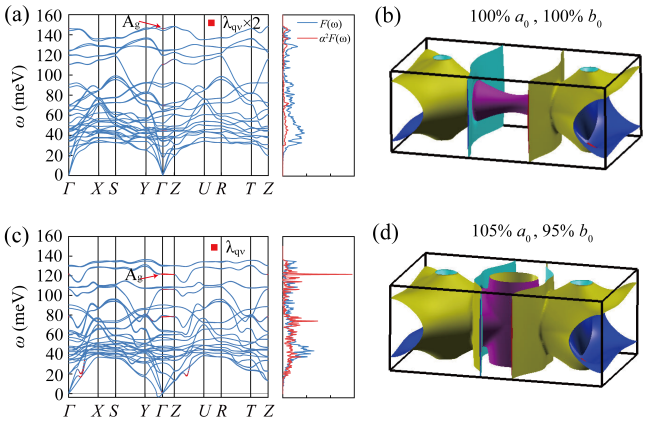


Fig. 5. (a) The phonon band dispersions and the corresponding EPC strengths $\lambda_{q\nu}$ for Li_2B_3C without strain, where the sizes of the red squares indicate the magnitudes of $\lambda_{q\nu}$. The sizes of squares are doubled in panel (a) for aesthetic visualization. The right subpanel displays the corresponding phonon DOS (blue curve) and the Eliashberg spectral function (red curve). (b) The Fermi surfaces for Li_2B_3C without strain. (c) The phonon band dispersions and the corresponding EPC strengths $\lambda_{q\nu}$ for Li_2B_3C under the optimal biaxial strain, where the sizes of the red squares indicate the magnitudes of $\lambda_{q\nu}$. The right subpanel displays the corresponding phonon DOS (blue curve) and the Eliashberg spectral function (red curve). (d) The Fermi surfaces for Li_2B_3C under the optimal biaxial strain.

The significant enhancement of the EPC originates from the significant change in the electronic structure. Figures 5(b) and 5(d) illustrate the reconstruction of Fermi surfaces. Under the optimal biaxial strain, the B–B bridge σ-bonding bands cross the Fermi level and the new elliptical cylindrical Fermi surfaces emerge around the Γ point. These new Fermi surfaces are composed of the states with larger deformation potentials, providing a dominant contribution to EPC. Moreover, these Fermi surfaces are even larger than those under the optimal uniaxial strain, therefore contributing a higher DOS at E_F. Given the relationship between deformation potential and total EPC strength[6,52–55] ($\lambda_{q\nu} = N(0)\frac{|D_{q\nu}|^2}{M_{q\nu}\omega_{q\nu}^2}$), this is also favorable for further enhancing the total EPC strength. Here $N(0)$ denotes the DOS at E_F, $D_{q\nu}$ denotes the shift in band energy resulting from a perturbation of the phonon mode $q\nu$ near the

Fermi level, M_{qv} is the averaged atomic mass, and ω_{qv} is the phonon frequency.

Figure 6(b) shows how the band structure is changed before and after introducing a perturbation on the lattice with an amplitude of 0.1 Å associated with the A_g phonon mode, consistent with our above discussion. The corresponding projected band structure and the projected DOS are depicted in Fig. 6(c). This provides a clear physical picture for its large deformation potential. Here we still select the A_g phonon mode as the representative bond-stretching phonon mode due to its strongest EPC. Its vibrational configuration (also the perturbation we introduce) is illustrated in Fig. 6(a), corresponding to the in-plane vibrations of boron and carbon atoms.

The deformation potential is proportional to the energy shift of electronic states at the Fermi level.[6,52] In our case, the B–B bridge σ-bonding band exhibits a pronounced downward energy shift after the perturbation at the Fermi level. In contrast, the π bands and the dispersive part of B–B zigzag chain σ-bonding bands are relatively unaffected. This is because the sensitive band maximum of the B–B bridge σ-bonding band lies only slightly above the Fermi level, as marked by the dashed purple circle in Fig. 6(c). Meanwhile, the band maximum of the B–B zigzag chain σ-bonding bands is far above the Fermi level, so these chain bands intersect the Fermi level via their insensitive dispersive portions. This is consistent with the directions of the perturbation in Fig. 6(a). Our perturbation contracts the bridge bonds, while elongating the chain bonds. This means the bridge bonds are strengthened and thus exhibit a larger bonding-antibonding energy splitting, while the chain bonds are weakened and with smaller bonding-antibonding energy splitting. Consequently, the top of the B–B bridge σ-bonding bands are lowered down while the top of B–B zigzag chain σ-bonding bands are lifted up and the dispersive parts remain nearly unaffected. Moreover, the π bands show weak changes, consistent with their reduced sensitivity to in-plane bond-stretching vibrations. Our analysis elucidates the origin of the strong EPC in biaxial-strained Li_2B_3C, which should also be applicable to other anisotropic structural modulations, such as uniaxial strain. Experimentally, such in-plane anisotropic strains can be realized by piezoelectric-based and mechanical strain devices.[50,51]

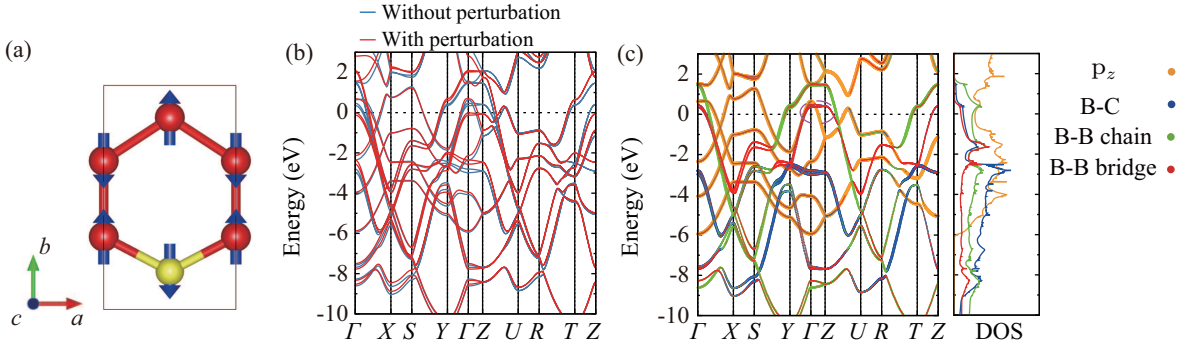


Fig. 6. (a) Illustration of the representative phonon mode with the strongest EPC, the A_g mode at Γ point, for Li_2B_3C under the optimal biaxial strain. Blue arrows indicate the directions of atomic displacements, while their lengths represent the relative amplitudes of the phonon mode. (b) Electronic band structure of Li_2B_3C under the optimal biaxial strain with a perturbation with an amplitude of 0.1 Å corresponding to the A_g phonon mode (red curve) compared to the band structure without perturbation (blue curve). (c) Projected band structure and DOS of Li_2B_3C under the optimal biaxial strain, highlighting the top of the σ-bonding bands near the Γ point, which is sensitive to phonon vibrations, marked by the dashed purple circle.

4. Conclusion

In summary, we present a systematic first-principles study to elucidate how biaxial strain manipulates the electronic structure and phonon-mediated superconductivity of Li_2B_3C. As a first step, we carry out structural optimizations and electronic structure calculations for all structures within the moderate biaxial strain range from -5% to $+5\%$. Inspired by our previous study,[31] we introduce a descriptor $\Delta\varepsilon$, defined as the energy difference between the B–B bridge σ-bonding band maximum and the Fermi level. Using $\Delta\varepsilon > 0.05$ eV as a screening criterion, we carry out EPC calculations and estimate T_c with the McMillan–Allen–Dynes formula. For all selected structures, T_c ranges from 14 K to 45 K. The maximum $T_c = 44.72$ K occurs at $+5\%$ a-axis strain and -5% b-axis strain, where the EPC is strongest ($\lambda = 1.13$) despite a slightly reduced logarithmic average phonon frequency ($\omega_{log} = 46.69$ meV).

We further show that b-axis compression or a-axis tension lifts up the B–B bridge σ-band maximum. TB parameters extracted from Wannierization reveal the microscopic mechanism of this tuning. On the one hand, such strain raises the on-site energy of the B–B bridge σ-bonding WF. On the other hand, such strain weakens the intra-chain hybridization but strengthens the bridge-chain hybridization. This is because $\theta_{1,2}$ decrease and $\theta_{3,4}$ increase under b-axis compressive or a-axis tensile strain. As a result, b-axis compression or a-axis tension broadens the B–B bridge σ-bonding band, facilitating the Lifshitz transition.

Finally, we study the EPC properties of the optimal biaxial-strained Li_2B_3C. Its strong EPC originates from the newly formed Γ-centered elliptical cylindrical Fermi surfaces.

Compared with the states from the dispersive part of σ-bonding band, these states, positioned near the B–B bridge σ-band maximum, are more sensitive to bond-stretching vibrations. Thus, these states have larger deformation potentials, leading to a pronounced contribution to EPC and an overall T_c enhancement. This study provides reliable theoretical guidance for tuning electronic structure and superconductivity by strain, and sheds new light on high-T_c superconductivity induced by metallic σ-bonding electrons.

Acknowledgments

Project supported by the National Natural Science Foundation of China (Grant Nos. 12404153 and 22276013) and the Fundamental Research Fund for the Central Universities (Grant No. FRF-TP-25-040). The calculations were done on Hefei advanced computing center and Taiyuan advanced computing center.

References

[1] Ashcroft N W 1968 *Phys. Rev. Lett.* **21** 1748
[2] Duan D, Liu Y, Tian F, Li D, Huang X, Zhao Z, Yu H, Liu B, Tian W and Cui T 2014 *Sci. Rep.* **4** 6968
[3] Drozdov A, Eremets M, Troyan I, Ksenofontov V and Shylin S I 2015 *Nature* **525** 73
[4] Peng F, Sun Y, Pickard C J, Needs R J, Wu Q and Ma Y 2017 *Phys. Rev. Lett.* **119** 107001
[5] Somayazulu M, Ahart M, Mishra A K, Geballe Z M, Baldini M, Meng Y, Struzhkin V V and Hemley R J 2019 *Phys. Rev. Lett.* **122** 027001
[6] An J M and Pickett W E 2001 *Phys. Rev. Lett.* **86** 4366
[7] Gao M, Lu Z Y and Xiang T 2015 *Physics* **44** 421 (in Chinese)
[8] Gao M, Lu Z Y and Xiang T 2015 *Phys. Rev. B* **91** 045132
[9] Zhang J F, Zhan B, Gao M, Liu K, Ren X, Lu Z Y and Xiang T 2023 *Phys. Rev. B* **108** 094519
[10] Nagamatsu J, Nakagawa N, Muranaka T, Zenitani Y and Akimitsu J 2001 *Nature* **410** 63
[11] Kortus J, Mazin I I, Belashchenko K D, Antropov V P and Boyer L L 2001 *Phys. Rev. Lett.* **86** 4656
[12] Rosner H, Kitaigorodsky A and Pickett W E 2002 *Phys. Rev. Lett.* **88** 127001
[13] Dewhurst J, Sharma S, Ambrosch-Draxl C and Johansson B 2003 *Phys. Rev. B* **68** 020504
[14] Miao R, Yang J, Jiang M, Zhang Q, Cai D, Fan C, Bai Z, Liu C, Wu F and Ma S 2013 *J. Appl. Phys.* **113** 133910
[15] Bazhirov T, Sakai Y, Saito S and Cohen M L 2014 *Phys. Rev. B* **89** 045136
[16] Li Q Z, Yan X W, Gao M and Wang J 2018 *Europhys. Lett.* **122** 47001
[17] Quan Y and Pickett W E 2020 *Phys. Rev. B* **102** 144504
[18] Liu H D, Wang B T, Fu Z G, Lu H Y and Zhang P 2024 *Phys. Rev. Res.* **6** 033241
[19] Yu W, Tang J H, Xu H R, Zhou G, Ouyang G, Deng H X, D'Agosta R and Yang K 2024 *New J. Phys.*
[20] Pickett W E 2006 *J. Supercond. Nov. Magn.* **19** 291
[21] Pickett W E 2017 arXiv:1801.00165 [cond-mat.supr-con]
[22] Bharathi A, Balaselvi S J, Premila M, Sairam T, Reddy G, Sundar C and Hariharan Y 2002 *Solid State Commun.* **124** 423
[23] Fogg A, Chalker P, Claridge J, Darling G and Rosseinsky M 2003 *Phys. Rev. B* **67** 245106
[24] Fogg A, Claridge J, Darling G and Rosseinsky M 2003 *Chem. Commun.* 1348
[25] Souptel D, Hossain Z, Behr G, Loser W and Geibel C 2003 *Solid State Commun.* **125** 17
[26] Zhao L, Klavins P and Liu K 2003 *J. Appl. Phys.* **93** 8653
[27] Nakamori Y and Orimo S I 2004 *J. Alloys Compd.* **370** L7
[28] Fogg A M, Meldrum J, Darling G R, Claridge J B and Rosseinsky M J 2006 *J. Am. Chem. Soc.* **128** 10043
[29] Burdett J K, Lee S and McLarnan T J 1985 *J. Am. Chem. Soc.* **107** 3083
[30] Miller G J 1998 *Eur. J. Inorg. Chem.* **1998** 523
[31] Gu Y, Hu J, Jiang H and Xiang T 2026 *Commun. Phys.* **9** 81
[32] Giannozzi P, Baroni S, Bonini N, Calandra M, Car R, Cavazzoni C, Ceresoli D, Chiarotti G L, Cococcioni M and Dabo I 2009 *J. Phys. Condens. Matter* **21** 395502
[33] Perdew J P, Burke K and Ernzerhof M 1996 *Phys. Rev. Lett.* **77** 3865
[34] Troullier N and Martins J L 1991 *Phys. Rev. B* **43** 1993
[35] Hamann D 2013 *Phys. Rev. B* **88** 085117
[36] Schlipf M and Gygi F 2015 *Comput. Phys. Commun.* **196** 36
[37] Marzari N, Vanderbilt D, De Vita A and Payne M 1999 *Phys. Rev. Lett.* **82** 3296
[38] Mostofi A A, Yates J R, Lee Y S, Souza I, Vanderbilt D and Marzari N 2008 *Comput. Phys. Commun.* **178** 685
[39] Marzari N, Mostofi A A, Yates J R, Souza I and Vanderbilt D 2012 *Rev. Mod. Phys.* **84** 1419
[40] Ponce S, Margine E R, Verdi C and Giustino F 2016 *Comput. Phys. Commun.* **209** 116
[41] Lee H, Ponce S, Bushick K, Hajinazar S, Lafuente-Bartolome J, Leveillee J, Lian C, Lihm J M, Macheda F, Mori H, Paudyal H, Sio W H, Tiwari S, Zacharias M, Zhang X, Bonini N, Kioupakis E, Margine E R and Giustino F 2023 *npj Comput. Mater.* **9**
[42] Allen P B 1972 *Phys. Rev. B* **6** 2577
[43] Allen P B and Dynes R C 1975 *Phys. Rev. B* **12** 905
[44] Baroni S, de Gironcoli S, Dal Corso A and Giannozzi P 2001 *Rev. Mod. Phys.* **73** 515
[45] Locquet J P, Perret J, Fompeyrine J, Mächler E, Seo J W and Van Tendeloo G 1998 *Nature* **394** 453
[46] Bozovic I, Logvenov G, Belca I, Narimbetov B and Sveklo I 2002 *Phys. Rev. Lett.* **89** 107001
[47] Johansson E, Tasnadi F, Ektarawong A, Rosen J and Alling B 2022 *J. Appl. Phys.* 131
[48] Yang Y, Yue T and Wang S 2022 *J. Phys. Condens. Matter* **34** 105601
[49] Liu Z, Li Q and Chen H 2024 *Phys. Rev. B* **110** 024105
[50] Chu J H, Analytis J G, De Greve K, McMahon P L, Islam Z, Yamamoto Y and Fisher I R 2010 *Science* **329** 824
[51] Worasaran T, Ikeda M S, Palmstrom J C, Straquadine J A, Kivelson S A and Fisher I R 2021 *Science* **372** 973
[52] Khan F and Allen P 1984 *Phys. Rev. B* **29** 3341
[53] Lee K W and Pickett W E 2004 *Phys. Rev. Lett.* **93** 237003
[54] Lee K W and Pickett W E 2005 *Phys. Rev. B* **72** 174505
[55] Tan H, Liu Y, Wang Z and Yan B 2021 *Phys. Rev. Lett.* **127** 046401